PHYSICAL REVIEW D VOLUME 17, NUMBER 1 1 JANUARY 1978

Measurement of the directional cosmic-ray muon range spectrum

W. R. Sheldon and J. R. Benbrook
Physics Department, University of Houston, Houston, Texas 77004

N. M. Duller and W. G. Cantrell*
Physics Department, Texas A&M University, College Station, Texas 78342

A. R. Bazer-Bachi, Gilbert Vedrenne, and Claude Dunet
Centre d'Etude Spatiale des Rayonnements, University of Toulouse, Toulouse, France
(Received 27 June 1977)

The French-U.S. muon experiment, operating in the Mt. Blanc Tunnel between France and Italy for six years, has yielded an extremely precise measurement of the depth–zenith-angle distribution of high-energy cosmic-ray muons. Data were obtained over the depth range of 700 to 5000 hg/cm^2 for zenith angles of 0° to 80° (except above 3400 hg/cm^2 where only the region of larger zenith angles was investigated). The absolute vertical-depth–intensity curve determined solely by this experiment is in general agreement with curves obtained by other authors using data from a variety of sources; however, significant differences can be noted. Comparison of the observed zenithal dependence to theoretical predictions indicates that muons are produced mostly from pion decay, with no evidence for direct muon production. The integral muon energy spectrum at sea level determined from the present underground measurements and Kobayakawa's range-energy relation is in agreement with other experiments, with an exponent $\beta = -2.45$.

I. INTRODUCTION

The muon intensity underground has been the subject of experimental investigations for some fifty years. These investigations have been concerned with problems in both high-energy astrophysics and elementary-particle interactions. The vertical-muon-depth–intensity curve is directly related to the primary cosmic-ray spectrum; its energy dependence and its constancy (or lack of constancy) in time and solar or sidereal coordinates need to be explained by suitable models for the acceleration and propagation of charged particles in the galaxy. Although an accurate determination of this curve is a very important aspect of underground muon measurements, the design of the present experiment was more strongly influenced by the need to obtain measurements which could be used to study high-energy interaction phenomena. The calculations of interest in this context[1-4] have shown that the intensity of secondary cosmic-ray muons, as a function of energy and zenith angle, while dependent on the spectrum and composition of the primary cosmic rays, also has a critical dependence on the dynamics of the interactions which create these energetic secondary particles. Since there were no measurements of the muon zenith-angle distribution suitable for comparison to the calculations, a French-U.S. collaborative experiment was undertaken for this purpose.

For this type of investigation it is important to make observations over a wide range of zenith angles since muons originating from different processes have different zenithal distributions. Conventional processes (decay of mesons, specifically pions and kaons) lead to the so-called "sec θ law" above a few hundred GeV (that is, more high-energy muons are incident from large zenith angles than from the vertical), while direct muon production (or muons from the decay of a very short-lived particle) yields a zenithal distribution which is nearly isotropic. A controversy was raised when measurements of muons above 1 TeV showed a flat zenithal distribution, indicating a large contribution from direct production, referred to by the authors as the *X process*.[5] It was not possible to resolve this question with magnetic-spectrometer measurements since results from even the largest spectrometers have large uncertainties at such high energies; additional underground muon measurements were needed to investigate the zenith-angle distribution over a larger range of angles and as a function of depth.

With these experimental requirements in mind, a French-U.S. collaboration was initiated and a muon detector was installed in the Mont Blanc Tunnel. This investigation had three principal objectives:

1. to establish a very accurate vertical-depth–intensity relation with a single detector at a single underground site;
2. to determine the angular distribution of muons as a function of depth; these results could then be compared to the calculated, model-dependent values[1-4] and with other experimental re-

sults[5];

3. to determine experimentally the muon range-energy relation by comparing the underground intensities to the absolute intensity and to the zenithal distribution[6] determined by magnetic spectrometers at the surface.

The Mont Blanc Tunnel was chosen as the experimental site for two reasons. First, the steep slopes of the mountain (~40°) allow a determination of the intensity at a given depth to be made over a wide range of zenith angles. The depth can be changed by moving the experiment to different garages in the tunnel. Garages are located every 300 m along the tunnel, and changes in the depth underground were facilitated by operating the experiment on a truck bed. The second reason for choosing this site is that the topography and geology of the location were extensively investigated prior to and during the drilling of the tunnel. Depths in hg/cm^2 of standard rock are known to better than 2%. This is probably the greatest precision that can be expected with an inhomogeneous absorber.

Goals 1 and 2 have been fulfilled and are reported here after a brief description of the experimental techniques. Available sea-level data are being evaluated for investigation of goal 3; this result will be presented at a later time.

II. DATA ACQUISITION AND REDUCTION

A. The experimental apparatus

A Geiger-counter hodoscope-telescope was used to collect the basic data. The experimental apparatus and data processing have been described in detail previously,[7] but the main characteristics are given below for convenience.

The trajectory of a muon is reconstructed by locating its position in each of three planes of crossed Geiger counters labeled top, middle, and low. An angular resolution of about one degree resulted from the use of counters of 3.95 cm diameter with a separation distance of 165 cm between the top and low planes. The total aperture was ±30°, with a total geometrical factor of 4400 cm^2 sr. Discrimination against the soft component was accomplished by placing a lead shield 10 cm thick between the middle and low trays and accepting only straight tracks as muons.

Muon events were sorted by computer analysis into a 47×47 event matrix, according to their arrival direction with respect to the axis of the telescope (the size of the event matrix is determined by the fact that there were 24×24 counters per tray). Not all recorded events were accepted as muons: bursts ($\lesssim$5%) and nonstraight tracks (< 10%) were not entered into the matrix since the former had indeterminate directions and the latter were most likely due to the soft component. The rates of nonmuon events were taken into account in the dead-time correction.[7]

The data were compiled in runs, each of which was associated with depth in the tunnel and a given direction for the telescope axis. Thus, to each bin of an event matrix there was associated a depth in hg/cm^2 of standard rock, a zenith angle, an azimuth angle, and an exposure (geometrical factor times corrected running time). A summary of data runs which have been analyzed is given in Table I. Measurements were made at three different locations in the tunnel, garages I, III, and V. The number of muons analyzed as a function of depth and zenith angle is illustrated in Fig. 1. Between 800 and 3400 hg/cm^2, almost the entire zenithal range between 0° and 80° has been investigated; beyond 3400 hg/cm^2 only the region of large zenith angles has been explored. Thus, up to 3400 hg/cm^2, the present data provide a basis for decoupling the effects of depth and zenith angle on the muon intensity. This is not the case for most underground measurements, where larger depths correspond to larger zenith angles.

The runs listed in Table I provide a total of 44 180 ($20 \times 47 \times 47$) statistically independent measurements. The numbers of counts recorded in many of these independent measurements are quite small. Since there is substantial overlap in the ranges of depth and zenith angle covered, the measurements have been combined into h and θ bins with associated average zenithal angle θ and depth $\bar{h}$ to facilitate computation of the muon intensity function. The size of the angular interval $\Delta\theta$ was set at 5°, and the depth interval Δh was allowed to increase with depth from 50 hg/cm^2 at $h = 1000$ hg-cm^2 to 100 hg/cm^2 at $h = 2500$ hg/cm^2. An iterative process was used to compute the $\bar{h}$ associated with a given bin. The details of this computation are presented in Appendix A.

B. The geometrical factor

The geometrical factor of the hodoscope-telescope has been computed using a Monte Carlo technique.[7] This calculation took the finite wall thickness of the counters into consideration and was based on the assumption that ten ion pairs were created on the average by a muon crossing a counter diameter, a value which had been determined by laboratory measurements of similar counters.[8]

Recent studies of the apparatus have shown that our initial determination of the geometrical factor was in error. Preliminary results from garages I and V revealed an anomalous dip of about 10%

TABLE I. Summary of data runs showing the Mont Blanc Tunnel garage in which the run was made, zenith angle θ_0 and azimuth ϕ_0 of the telescope axis, zenithal $\langle\theta_0\rangle$ and depth $\langle h\rangle$ range investigated, calendar period of the run (in the form day/month/year) corrected time (Ref. 7) T_m of the run, total number of events N_E, and number for muons N_μ per run.

Garage	θ_0	ϕ_0	$\langle\theta_0\rangle$	$\langle h\rangle$ (hg/cm^2)	Period	T_m (10^6 sec)	N_E	N_μ	N_μ/N_E
I	0°	144.6°	0–32°	750–1400	7/68–8/68	4.750	3 820	3 325	0.87
I	0°	144.6°	0–32°	750–1400	8/68–15/2/69	4.750	37 298	33 096	0.888
I	63°	144.6°	45–80°	750–1400	15/2/69–5/5/69	1.680	20 660	18 530	0.897
V	61°	122.5°	42–82°	2500–6500	7/6/69–13/12/69	1.263	247	212	0.858
V	15°	122.5°	0–40°	2500–3600	14/12/69–15/6/70	10.76	2 517	2 234	0.887
V	63°	122.0°	44–84°	2500–6400	15/9/70–17/6/71	21.37	4 009	3 559	0.888
V	65°	300°	45–85°	7500–12 000	18/6/71–4/7/71	1.47	5	0	0
III	0°	141.4°	0–30°	1600–2400	10/8/71–17/3/72	11.591	8 888	7 716	0.868
III	67°	141.4°	46–87°	1600–4500	18/3/72–15/4/72	1.782	2 042	1 780	0.872
III	67°	141.4°	46–87°	1600–4500	18/2/73–19/6/73	8.444	9 756	8 567	0.878
III	35°	141.4°	5–60°	1600–2100	20/6/73–26/4/74	16.067	23 362	20 680	0.885
III	15°	141.4°	0–45°	1600–2300	27/4/74–16/6/74	3.426	3 876	3 378	0.872
I	0°	137.5°	0–32°	750–1450	26/6/74–17/7/74	1.405	12 195	10 395	0.852
I	0°	137.5°	0–32°	750–1450	17/7/74–5/8/74	0.6277	4 896	4 313	0.880
I	0°	137.5°	0–32°	750–1450	6/8/74–12/10/74	2.136	16 158	14 315	0.885
I	10°	137.5°	0–40°	750–1200	12/10/74–17/11/74	1.891	18 477	16 613	0.899
I	20°	137.5°	0–50°	750–1100	17/11/74–18/12/74	1.533	17 762	16 003	0.901
I	31°	137.5°	3–60°	750–1300	6/1/75–6/2/75	1.376	17 745	15 152	0.899
I	61°	137.5°	40–78°	780–1450	6/2/75–8/3/75	1.716	13 278	17 426	0.904
I	70°	137.5°	45–78°	780–1450	8/3/75–25/3/75	0.856	6 772	6 080	0.890

in the angular distribution at around 30°.[9] However, data in this zenith-angle region resulted exclusively from muons arriving at large angles to the telescope axis, and instrumental effects were suspected.

In order to investigate the anomalous dip at ~30°, runs were made during 1974–1975 in garage I at zenith angles of 0°, 10°, 20°, and 30° (see Table I). When data from only the portion of the telescope near the axis were analyzed, the dip was not present, and thus the suspected error in the initial data analysis was confirmed.[10] Since a large number of counts were accumulated during this phase of the experiment with a given direction being viewed by different parts of the telescope aperture, these data provide the basis for an experimental determination of the geometrical factor. The anomalous dip at 30° was presumed to be due to an overestimation of the geometrical factor of telescope elements farthest from the axis. The Monte Carlo calculation of the geometrical factor was repeated using a lower value for muon ionization efficiency, and a good fit to the measured values was obtained by assuming that eight ion pairs instead of ten were created per muon traversal of a counter diameter. The overall geometrical factor was decreased by less than 1% from the value reported

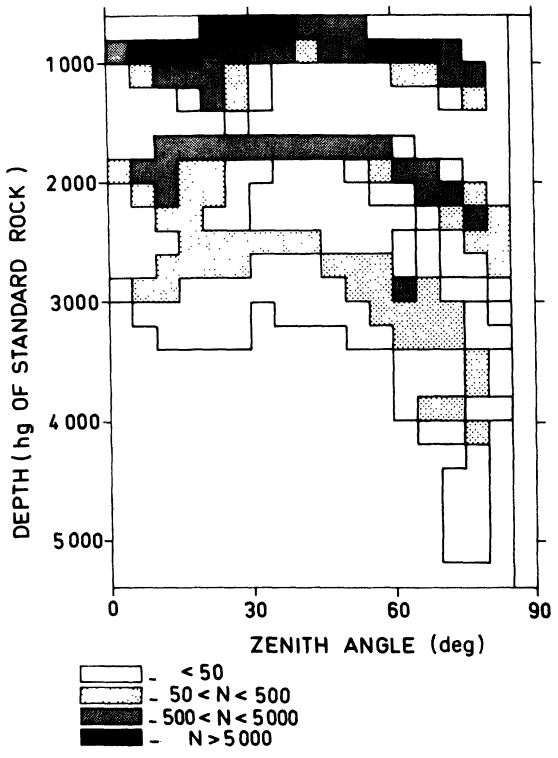

FIG. 1. Distribution of the experimental data as total counts per interval of depth and zenith angle.

previously,[7] but the effect was as high as 10% for directions far from the axis.

C. Data analysis

A representation of the muon intensity in terms of depth and zenith angle which takes all of the physical processes into account cannot be presented in terms of a simple analytical expression. Too many convolutions of various origin are involved in the transition from primary particles to muons underground. In general, two types of expressions are used as fitting functions for underground muon data (results of the present experiment have been analyzed using both).

(1) The first type is an empirical function based on approximations to physical phenomena; a well-known example is the Miyake representation[11]:

$$I_M(\theta,h) = \frac{A}{h\cos\theta + B}(h + 9\sec\theta)^{-\alpha}\frac{h+75}{h+50+25\sec\theta} \times \exp[-\beta(h+9\sec\theta)]. \quad (1)$$

This formula (modified here for the characteristics of the Mont Blanc experiment) implies a conventional origin for muons and does not allow for the possible presence of fine structure.

(2) The second type is a less restrictive, parametrized function of depth and zenith angle to simply fit the data; the resulting fitted functions are then compared with curves which have been computed numerically for various models of primary spectra, high-energy interactions, and propagation of muons to the telescope. From this kind of comparison it is possible to determine the relative effects of various physical parameters of the models. Such a general function can be of any type. However, since intensity is known to follow roughly a power law in depth, and the angular dependence is known to vary approximately as $(\sec\theta)^n$, we have used the following expression to fit the data:

$$I_h(\theta,h) = G(\sec\theta)^{a(\theta,h)}h^{b(\theta,h)}, \quad (2)$$

where G is a constant and $a(\theta,h)$ and $b(\theta,h)$ are polynomial expansions in $\ln h$ and $\ln\sec\theta$. Equation (2) can also be written

$$\ln I_h(\theta,h) = \sum_{i=0}^{n}\sum_{j=0}^{n} A_{ij}\left(\ln\frac{h}{h_0}\right)^i(\ln\sec\theta)^j. \quad (3)$$

And since the theoretical models are derived in terms of muon energy at sea level, in order to compare the experimental to the theoretical results, it is necessary either to extend the theoretical work to expressions in depth underground or to transform the dependence of the experimental results from depth to sea-level muon energy. We have chosen the latter by rewriting Eq. (2):

$$I_E(\theta,E) = 1_0(\sec\theta)^{c(\theta,E)}E^{d(\theta,E)}. \quad (4)$$

Depth can be substituted for energy by use of the energy-loss relation

$$-\frac{dE}{dh} = a(E) + b(E)E. \quad (5)$$

Kobayakawa[12] has shown that this can be simply integrated to give

$$E = \frac{a_{\rm eff}}{b_{\rm eff}}[\exp(b_{\rm eff}h) - 1], \quad (6)$$

where $a_{\rm eff}$ and $b_{\rm eff}$ are functions of E, slightly different from a and b in (5). Moreover, one can consider $a_{\rm eff}$ and $b_{\rm eff}$ to be constant over the depth range involved here, so that relation (4) becomes

$$\ln I_E(\theta,h) = \sum_{i=0}^{n}\sum_{j=0}^{m} C_{ij}[\ln(e^{bh}-1)]^i(\ln\sec\theta)^j. \quad (7)$$

A value of $b = 3.6\times10^{-6}$ cm^2/g was used in Eq. (7).

III. DEPTH AND ZENITH ANGLE

The analysis has been performed using the three functions defined above, I_M, I_h, and I_E. These functions were fitted to the data by the method of χ^2 minimization and by the maximum-liklihood technique. In all cases, differences between the results obtained by the two methods were small. The results given below are those obtained from the maximum-likelihood technique, and the details of how this method was adapted to the analysis of the present experiment are given in Appendix B.

Data were first analyzed run by run, then for each garage, and finally as a whole. Independent runs showed good consistency in overlapping regions. Measurements in garage I made in 1974–1975 gave the same absolute intensities as those obtained in 1968–1969, thus indicating that the detector efficiency has not changed with time. The whole set of data was combined into 756 $(\Delta h, \Delta\theta)$ bins (Appendix A). The results obtained by fitting each of the functions I_M, I_h, and I_E to the data are discussed below.

(i) *Fit to Miyake's function.* The set of four coefficients is the following:

$$M_1 = A = 206 \pm 35,$$
$$M_2 = B = 348 \pm 10,$$
$$M_3 = \alpha = -1.60 \pm 0.03,$$
$$M_4 = \beta = (6.13 \pm 0.17)\times10^{-4},$$

with the associated error matrix:

$$\langle \Delta M_i \Delta M_j \rangle = \begin{bmatrix} -0.124\times 10^{4} & -0.928\times 10^{2} & -0.943 & 0.580\times 10^{-3} \\ -0.928\times 10^{2} & -0.104\times 10^{3} & -0.522\times 10^{-1} & 0.669\times 10^{-5} \\ -0.943 & -0.522\times 10^{-1} & -0.724\times 10^{-3} & 0.453\times 10^{-6} \\ 0.580\times 10^{-3} & 0.669\times 10^{-5} & 0.453\times 10^{-6} & 0.308\times 10^{-9} \end{bmatrix}.$$

The uncertainty in $I_M(\theta, h)$ is given by

$$[\Delta I_M(\theta, h)]^2 = \sum_{i,j} \langle \Delta M_i \Delta M_j \rangle \frac{\partial I_M}{\partial M_i} \frac{\partial I_M}{\partial M_j}.$$

The resulting errors are smaller than 1% over most of the range.

(ii) *Fit to relations (3) and (7).* Fits have been made with sets of coefficients ranging from 2×2 to 7×7. (The first number gives the degree in $\ln \sec\theta$, the second in $\ln h$.) Of course, increasing the number of coefficients will produce better fits to the actual data points; however, the function may exhibit unphysical excursions between data points and beyond the data if the degree is too high. Thus, one must balance the two effects. It was found that a 3×4 set of coefficients, using Eq. (7), yields a good fit to the data and a good overall behavior. The coefficients to determine the intensity in units of 10^{-8} cm^{-2} sr^{-1} sec^{-1} are given in Table II and the error matrix is given in Table III, taking advantage of the symmetry property of this matrix. Table IV presents values of muon intensity at several values of zenith angle and depth (and the corresponding calculated energies) which have been computed from the coefficients of Table II.

The vertical-depth–intensity curve derived from the above set of coefficients is shown in Fig. 2, for h in the range 500 to 5000 hg/cm^2 of standard rock. Uncertainties indicated by the dashed line are statistical only; an uncertainty in depth of $\lesssim 2\%$ has not been included.

We have compared this vertical-depth spectrum with recent compilations given by several authors, as shown in Fig. 3. Here Miyake's curve[11] has been converted to standard rock. (Miyake's curve for Kolar gold field (KGF) is also shown by Krishnaswamy *et al.*,[13] along with their KGF results and those of other experiments.) Also plotted in Fig. 3 are the world-survey depth-intensity curve of Cassiday[14] and the compilation given by Wright.[15] These curves have uncertainties of about 10% and are not in agreement over most of the 500–5000-hg/cm^2 range, although they share in part the same original set of data. The Utah vertical points[16] are in much closer agreement with our result. The vertical-range spectrum reported here has an accuracy of ±3%, including all effects, from 800 to 3400 hg/cm^2. We believe that the only way to further improve this accuracy would be to perform measurements under water, since a determination of depth over large ranges of inhomogeneous overburdens to better than 1% is probably not attainable.

The vertical-range spectrum of Fig. 2 is based upon knowledge not only of the intensity at 0° zenith angle, but also from that at other angles. Data close to the vertical are available only up to 3000 hg/cm^2; however, the data at large zenith angles and the observed zenithal dependence allow an extropolation to be made up to 5000 hg/cm^2.

We shall now turn to the overall angular distribution. A way to investigate the zenith-angle dependence as a function of depth is to examine the enhancements, $I(\theta, h)/I(0°, h)$. We have used the calculations of Cantrell[4] for conventional and directly produced muons to compare to our data. Figures 4 and 5 give cross sections of the depth–zenith-angle surface. Our aim here is to evaluate the predictions of the various interaction models. Differences between the models are more easily seen at greater depths and larger zenith angles, where differences in predicted enhancements become very distinct. The figures show the enhancements expected from a 100% pion source (curve A), an 80%π-20%K mixture (curve B), and an addition of 2% direct production to the 80%-20% mixture. Clearly, our data do not support, by several stan-

TABLE II. Coefficients for Eq. (7) with the associated uncertainty obtained by fitting the data of the present experiment (see Appendix B). Table I and Fig. 1 should be consulted when using these coefficients since they are applicable only within the realm of the data.

i	j	C_{ij}	ΔC_{ij}
0	0	2.7107	8.4×10^{-3}
0	1	0.972	0.037
0	2	−0.271	0.030
1	0	−2.525	0.021
1	1	0.39	0.10
1	2	−0.20	0.07
2	0	−0.05	0.01
2	1	−0.11	0.08
2	2	0.14	0.07
3	0	−0.048	0.015
3	1	−0.046	0.1
3	2	−0.004	0.07

TABLE III. Error matrix for the coefficients of Eq. (7) obtained in the fitting procedure described in Appendix B. Since the matrix is symmetric, redundant terms are not shown.

i	j	0 0	0 1	0 2	1 0	1 1	1 2	2 0	2 1	2 2	3 0	3 1	3 2
0	0	-0.705×10^{-4}											
0	1	0.220×10^{-3}	-0.139×10^{-2}										
0	2	-0.128×10^{-3}	0.106×10^{-2}	-0.916×10^{-3}									
1	0	-0.770×10^{-4}	0.145×10^{-3}	-0.413×10^{-4}	-0.461×10^{-3}								
1	1	0.753×10^{-4}	-0.416×10^{-3}	0.272×10^{-3}	0.135×10^{-2}	-0.107×10^{-1}							
1	2	0.716×10^{-5}	-0.104×10^{-3}	0.240×10^{-3}	-0.757×10^{-3}	0.685×10^{-2}	-0.516×10^{-2}						
2	0	0.349×10^{-4}	-0.143×10^{-3}	0.103×10^{-3}	-0.102×10^{-3}	0.425×10^{-3}	-0.291×10^{-3}	-0.130×10^{-3}					
2	1	-0.161×10^{-3}	0.182×10^{-2}	-0.165×10^{-2}	0.226×10^{-3}	0.487×10^{-3}	0.701×10^{-3}	0.364×10^{-3}	-0.648×10^{-2}				
2	2	0.109×10^{-3}	-0.155×10^{-2}	0.161×10^{-2}	-0.145×10^{-3}	-0.951×10^{-3}	-0.644×10^{-3}	-0.230×10^{-3}	0.571×10^{-2}	-0.558×10^{-2}			
3	0	0.390×10^{-4}	-0.515×10^{-4}	0.483×10^{-5}	0.267×10^{-3}	-0.811×10^{-3}	0.478×10^{-3}	0.153×10^{-4}	-0.975×10^{-4}	0.106×10^{-3}	-0.210×10^{-3}		
3	1	-0.168×10^{-4}	0.596×10^{-3}	-0.499×10^{-3}	-0.993×10^{-3}	0.956×10^{-2}	-0.592×10^{-2}	-0.256×10^{-3}	-0.356×10^{-2}	0.331×10^{-2}	0.714×10^{-3}	-0.113×10^{-1}	
3	2	-0.249×10^{-4}	0.412×10^{-4}	-0.123×10^{-3}	0.598×10^{-3}	-0.590×10^{-2}	0.441×10^{-2}	0.215×10^{-3}	0.120×10^{-2}	-0.774×10^{-3}	-0.442×10^{-3}	0.695×10^{-2}	-0.519×10^{-2}

dard deviations, a significant contribution from nonconventional sources. This confirms the more recent Utah results.[16] We can give an upper limit of 0.5% for direct muon production below 3 TeV.

It is somewhat more difficult to determine a precise value of the π/K ratio from the present data. Certainly, most of the data support a high percentage of pions. This is in agreement with predictions from scaling. It can be noted that the enhancements do not behave as predicted at 80°, being generally lower. This is probably due to the paucity of data in that angular range and the effect of a neighboring mountain which occults muons arriving from directions near the horizon.[7,17]

Another hindrance to a precise measurement of the π/K ratio lies in the theoretical calculations themselves. Variations in the incoming primary spectrum, the dynamics of the interactions, and the mean free paths for different particles involved can result in enhancements which differ by up to 30%, according to various authors. The need remains for a precise calculation of this ratio, taking all known effects into account.

IV. THE ENERGY SPECTRUM

The depth-intensity relation can be converted into a sea-level muon energy spectrum. We have used the results of Kabayakawa[12] for the range-energy relation and for the fluctuation correction factor, R. This latter is a function of β, the exponent of the muon energy spectrum at sea level, so an iterative process was used. First, a constant β value of -2.5 was arbitrarily chosen to obtain $R(h)$. This $R(h)$ and the measured range spectrum produced a calculated surface energy spectrum with an energy-dependent exponent. This new surface spectrum led to a new $R(h)$, and so on. After two iterations, the variation in the calculated energy spectrum became smaller than 1 standard deviation, and the process was terminated.

The data (intensity versus energy) were fitted to a power law, first with constant index:

$$I(>E) = AE^{\beta} .$$

With E expressed in TeV, the maximum-likelihood method gave the following result:

$$A = (5.686 \pm 0.023)\times 10^{-8} ,$$

$$\beta = -2.453 \pm 0.005 .$$

Now, letting β vary with energy, $\beta = \beta_0 + \lambda \ln E$, with E again in TeV, we get

$$A = (5.767 \pm 0.03)\times 10^{-8} ,$$

$$\beta_0 = -2.469 \pm 0.006 ,$$

$$\lambda = -2.029 \pm 0.006 .$$

TABLE IV. The directional muon underground intensity in counts $cm^{-2}sec^{-1}sr^{-1}$ for zenithal directions for the vertical to 80°. These intensities are computed from the coefficients of Table II.

E (GeV)	h (hg/cm^2)	0°	30°	45°	60°	70°	75°	80°
100	388	2.110×10^{-5}	2.185×10^{-5}	2.400×10^{-5}	3.184×10^{-5}	5.177×10^{-5}	8.317×10^{-5}	1.950×10^{-4}
200	729	3.191×10^{-6}	3.404×10^{-6}	3.776×10^{-6}	4.666×10^{-6}	6.181×10^{-6}	7.853×10^{-6}	1.162×10^{-5}
400	1306	5.435×10^{-7}	6.038×10^{-7}	6.938×10^{-7}	8.581×10^{-7}	1.044×10^{-6}	1.178×10^{-6}	1.350×10^{-6}
600	1783	1.962×10^{-7}	2.231×10^{-7}	2.628×10^{-7}	3.317×10^{-7}	3.997×10^{-7}	4.379×10^{-7}	4.667×10^{-7}
800	2190	9.467×10^{-8}	1.092×10^{-7}	1.309×10^{-7}	1.682×10^{-7}	2.037×10^{-7}	2.218×10^{-7}	2.308×10^{-7}
1000	2545	5.335×10^{-8}	6.215×10^{-8}	7.531×10^{-8}	9.823×10^{-8}	1.200×10^{-7}	1.309×10^{-7}	1.355×10^{-7}
1500	3274	1.826×10^{-8}	2.152×10^{-8}	2.648×10^{-8}	3.536×10^{-8}	4.416×10^{-8}	4.881×10^{-8}	5.134×10^{-8}
2000	3851	8.265×10^{-9}	9.765×10^{-9}	1.207×10^{-8}	1.630×10^{-8}	2.070×10^{-8}	2.323×10^{-8}	2.508×10^{-8}

Figure 6 shows a curve obtained from these values. The fit which includes the steepening spectrum, as indicated by the negative value of λ, is much closer to the data than is the case for any constant β. The indicated error has two sources. The first is due to statistical uncertainty and depth error in the depth-intensity relation and is of the order of 5% over most of the range. The second source of error is related to the uncertainty in converting from range to energy and in the correction factor, R. This second part is harder to evaluate, since theoretical calculations are the only available guide. However, an estimate made by Kobayakawa[12] has been included in the figure.

Finally it can be noted that the data are even better represented by a piecewise fit, using a compound power law with constant exponents, the transition occuring just above 1 TeV; below, the exponent is −2.4, and above, −2.65.

A steepening muon spectrum is predicted by calculations based on a primary spectrum with a constant exponent such as that of Magnuson *et al.*[18] and a steepening primary spectrum at around 10 TeV would increase this effect. The observed change in slope is rather small and does not strongly support such a change in the primary spectrum.

It has been noted by Kitamura[19] that the sea-level muon energy spectrum derived from underground data is in good agreement with determinations made using other techniques. The present result is a confirmation of that conclusion.

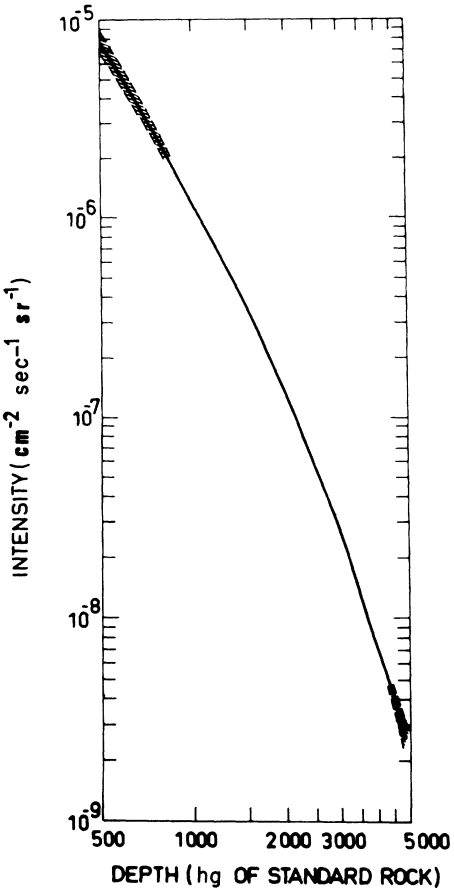

FIG. 2. The vertical-depth–intensity relation of the present experiment. The dashed lines at either end of the curve indicate 1 standard deviation of statistical uncertainty determined only from the counting rate.

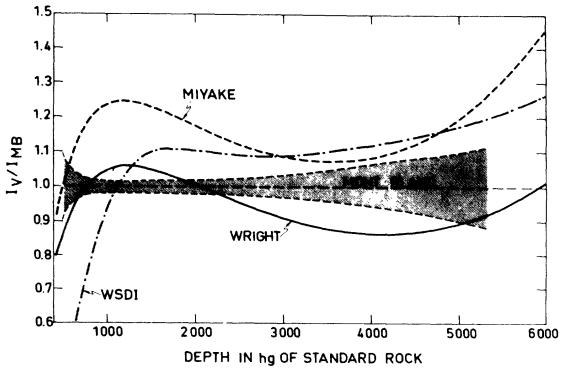

FIG. 3. Comparison of other vertical muon spectra to the present experiment. The shaded region represents the statistical uncertainty in the present experiment as in Fig. 2.

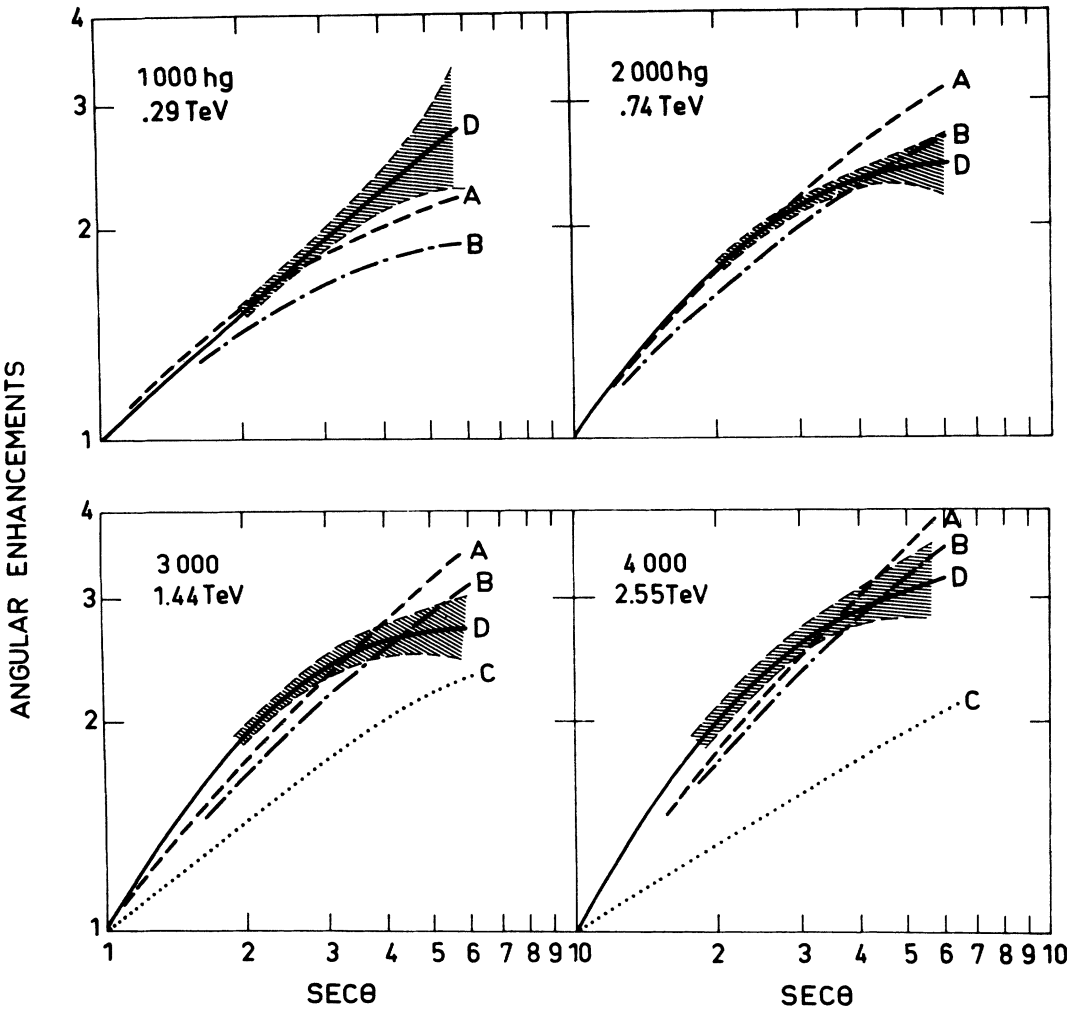

FIG. 4. Angular enhancements as a function of zenith angle at four depths underground. Curve A is the calculated enhancement assuming all of the underground muons arise from pion decay; B includes a 20% contribution from kaon decay; and C is for a 2% direct (or X-) production contribution to the 80% pion+20% kaon model. Curve D is the result from the present experiment, with the shaded area representing the statistical uncertainty as in Figs. 2 and 3.

V. DISCUSSION

The vertical-depth–intensity curve of cosmic-ray muons has been studied by a number of workers,[11,14,15,20,21] who used, for the most part, the same body of data. However, significant differences in their curves can be noted, largely due to differences in normalization, weighting of various data sets, curve-fitting techniques, etc. By contrast, the vertical curve, Fig. 2, of the present experiment is an absolute measurement based only on the present data.

The burden which is assumed by this experiment in making such a claim is that absorber thicknesses of the overlying rock at the site and the counting efficiency of the telescope are accurately known. The accuracy to which the composition and topography of the overburden are known has been discussed previously.[7] It should be noted that the determination of the average depth associated with a particular bin of the data made full use of the available depth information, including the 1° resolution of the telescope and the experimental dependence of the intensity on depth (Appendix A). An accurate knowledge of the counting efficiency requires that (1) the efficiency with which particles other than muons are rejected, and (2) the efficiency for counting a beam of energetic muons be known. Over the range of depths investigated here, it is important to reject the flux of secondary electrons in equilibrium with the muons. The efficiency with which electrons were rejected is

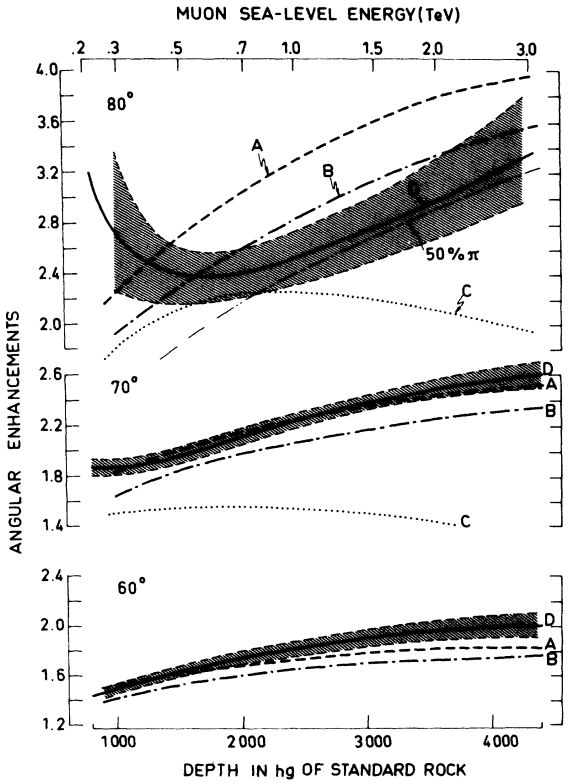

FIG. 5. Angular enhancements as a function of depth for zenith angles of 60°, 70°, and 80°. Curves A, B, C, and D are as described for Fig. 4. A curve calculated for a 50% pion + 50% kaon source for the muons is shown for 80°.

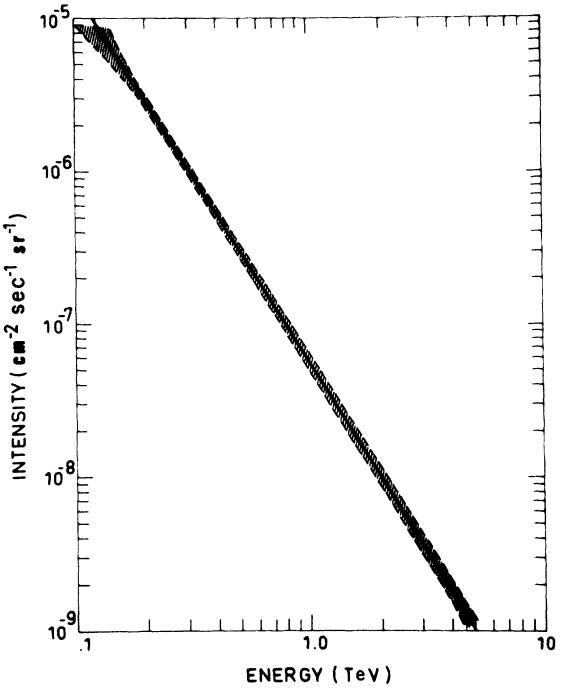

FIG. 6. The vertical sea-level muon energy spectrum determined from the underground data of the present experiment and Kobayakaya's range-energy relation. The shaded area indicates the uncertainty from all sources.

demonstrated by the fact that the shadow of a neighboring mountain appeared in the data[7,17]; electrons would not maintain trajectories related to this shadow, and since no events contaminate the shadow region, it is concluded that electron events have been removed from all of the data. Regarding (2), the efficiency with which a beam of muons is counted by the telescope is included in the Monte Carlo calculation of the geometrical factor by applying Poisson statistics to determine the number of ion pairs created in a single counter by the traversal of a muon. As discussed previously herein, the mean number of ion pairs created by a muon crossing the diameter of a counter was determined to be 8, rather than 10, in order to yield consistent measurements. With this correction the resulting efficiency of the telescope, when corrected for the background counting rate[7] has been very accurately determined.

The purpose of using a telescope which could be rotated to investigate various zenithal directions was to ensure that at least the *relative* zenithal variation would be measured. However, this ability to change the pointing direction of the telescope axis has facilitated a detailed investigation of the properties of the instrument itself and hence an *absolute* measurement of the muon directional range spectrum has been obtained.

The investigation of angular enhancements (Figs. 4 and 5) is a comparison of directional muon intensities measured underground to calculations of the directional muon flux in the atmosphere. An assumption which is implicit in this comparison is that the directions of energetic muons are not changed significantly in traversing large thicknesses of absorber. The observation of the shadow of the neighboring mountain, noted above, indicates that this is the case and also demonstrates that low-energy muons are removed from the data. These low-energy particles are absorbed by the lead shield or scattered into nonstraight trajectories which are rejected during the analysis.

Another indication of the directional properties of the telescope can be seen by the last data run in garage V shown in Table I. The azimuth of the telescope was changed during this run so that the average depth was increased by a factor of ~4. In the eighteen-day run at this depth, no muon counts were expected and none were measured. Five spurious events were detected during this time, but were rejected during routine analysis of the data.

The time associated with each muon event was recorded, so that it is possible to analyze the present data in terms of arrival direction in celestial coordinates; a preliminary analysis has been presented elsewhere.[22]

VI. CONCLUSION

The French-U.S. cosmic-ray experiment in the Mont Blanc tunnel provides measurements of underground muon intensities with sufficient accuracy to be useful as calibration standards over most of the depth range from 500 to 4000 hg/cm^2 of standard rock and at zenith angles from the vertical down to 80°. The range in depth of this experiment corresponds to muon sea-level energies ~100 GeV–5 TeV. The present results are in general agreement with other comprehensive underground muon experiments and collated surveys, but significant differences exist. The general disagreement among authors in the vertical intensity at around 500 hg/cm^2 should be noted; more careful experiments in this depth region seem to be suggested.

Greater precision over much of the depth and zenith-angle regions covered by this experiment can be had only at considerable expense and would appear to be of only marginal added value (except for studies of time variations). The present results are more than adequate for conclusive studies of the important current questions which can be answered by comparison to theoretical models of muons in the atmosphere in the energy range covered here. It appears that the general methods and design of the present experiment will be the first approach to take when crucial new issues arise which can be resolved by deep underground muon intensity measurements. Of course, accurate experimental results at greater depths than those reported here are of immediate interest.

ACKNOWLEDGMENTS

The authors wish to express their thanks to the many people who have contributed to this experiment. We are very indebted to Mr. Dennis Barber for the help provided during the construction of the electronics. Messrs. Sanitas and St. Marc assisted in installing the apparatus, and Messrs. Coutelier, Chevassut, and Landé, in operating it. We are very grateful to Professor R. Maze and his staff from the Laboratoire de Physique Cosmique for providing the counters. The Societé du Tunnel sous le Mont-Blanc kindly provided the experimental site, and we thank M. Arnaud for his cooperation. Information on the geology of the site was provided partly by Professor Ouliannoff of the University of Lausanne, and in great detail by the Bureau des Recherches Geologiques et Minieres at Lyon, and we thank M. Gudefin of the BRGM for his kind assistance. For his encouragement it is a pleasure to thank Professor Francis Cambou. This research was supported in part by the Centre National de la Recherche Scientifique (CNRS) of France and by NASA Contract No. NAS9-14209 of the USA.

APPENDIX A: CALCULATION OF AVERAGE DEPTH AND ANGLE

The data in the 47 × 47 event matrices from each of the 20 runs were regrouped into bins of size $\Delta\theta$ and Δh in zenith angle and depth, respectively. Associated with each bin was an average angle $\bar{\theta}$ and an average depth $\bar{h}$. The value used for $\bar{\theta}$ was the midpoint of the 5°-wide bin. The value of $\bar{h}$ for a given bin was calculated as a weighted average of the h's associated with the individual event matrix elements contributing to the bin. The weighting method utilized the fact that over a limited range of depth Δh the intensity variation with h can be expressed by

$$I(h) = I_0 h^{\alpha}, \tag{A1}$$

where α = constant. Let I_i be the intensity from one of the contributing event matrix elements, h_i be the depth, N_i be the counts, and F_i be the exposure associated with the element. Then

$$I_i = N_i / F_i, \tag{A2}$$

and the ratio of intensities from two such elements is

$$\frac{I_i}{I_j} = \frac{N_i F_j}{N_j F_i} = \frac{h_i^{\alpha}}{h_j^{\alpha}}. \tag{A3}$$

Thus,

$$\frac{N_i}{N_j} = \frac{F_i h_i^{\alpha}}{F_j h_j^{\alpha}}. \tag{A4}$$

The average intensity obtained from the n contributing matrix elements in the Δh range,

$$\bar{I} = \sum_{i=1}^{n} N_i \Big/ \sum_{i=1}^{n} F_i = I_0 \bar{h}^{\alpha}, \tag{A5}$$

then defines the average depth, $\bar{h}$. Equations (A1) through (A4) can be used to obtain the result

$$\bar{h}^{\alpha} = \sum_{i=1}^{n} F_i h_i^{\alpha} \Big/ \sum_{i=1}^{n} F_i. \tag{A6}$$

The values of $\bar{h}$ associated with the bins were then calculated from (A6) in an iterative process. A value of $\alpha = -3.5$ was used to obtain a first set of $\bar{h}$'s. These values were used to fit the data to Eq. (3) and the resulting values of $\alpha(h)$ were used to calculate a new set of h's. Subsequent iterations

were deemed unnecessary since the corrections to the h's were much smaller than the errors associated with the h_i's.

APPENDIX B: MAXIMUM-LIKELIHOOD ANALYSIS

The data accumulated in a given bin consist of counts obtained from a stochastic source. The appropriate probability density function to use in describing the data is thus the Poisson distribution. The probability of counting N_i events in the ith bin is

$$P_{M_i}(N_i) = \frac{M_i^{N_i}}{(N_i)!} e^{-M_i},$$

where M_i is the mean number of counts appropriate for the bin. The objective is to derive from the data some analytic expression for the intensity, $I(h_i, \theta_i, C_j)$, where the C_j are the p constants that determine the function I. With this expression for the intensity, the mean number of counts for the ith bin is

$$M_i = F_i I(\bar{h}_i, \bar{\theta}_i; C_j),$$

where F_i is the exposure associated with the ith bin (geometrical factor times corrected running time) and $I(\bar{h}_i, \bar{\theta}_i)$ is the intensity at depth h_i and zenith angle $\bar{\theta}$.

The probability of observing N_i counts in the ith bin is then

$$P_{M_i}(N_i) = \frac{[F_i I(h_i, \theta_i; C_j)]^{N_i}}{(N_i)!} \exp[-F_i I(\bar{h}_i, \bar{\theta}_i; C_j)].$$

The likelihood function[23] for the n bins of the experiment is defined as

$$L = \prod_{i=1}^{n} P_{M_i}(N_i),$$

and the best choice of parameters C_j is that set C_j which maximizes L. Since maximizing L is equivalent to maximizing w, where

$$w = \ln L = \sum_{i=1}^{n} \ln[P_{M_i}(N_i)],$$

the problem of determining the optimum set C_j is reduced to solving the system of equations.

$$\frac{\partial w}{\partial C_j} = 0, \quad j = 1, \ldots, p.$$

Since

$$w = \sum_{i=1}^{n} N_i \ln[I(\bar{h}_i, \bar{\theta}_i; C_j)] - F_i I(\bar{h}_i, \bar{\theta}_i; C_j) + \text{constants},$$

then

$$\frac{\partial w}{\partial C_j} = \sum_{i=1}^{n} [N_i - F_i I(\bar{h}_i, \bar{\theta}_i; C_j)] \times \frac{\partial}{\partial C_j} \ln[I(\bar{h}_i, \bar{\theta}_i; C_j)] = 0$$

is the system of equations to be solved. The representations for I presented in Sec. II of this paper make the equations nonlinear, and the optimum set C_j must be obtained by an iterative numerical method. The multidimensional Newton-Raphson technique was used, and the iteration equations were expressed as

$$C_{j_{m+1}} = C_{j_m} + \sum_{k} H_{jk}^{-1} \frac{\partial w}{\partial c_k},$$

where

$$H_{jk} = -\frac{\partial^2 w}{\partial C_j \partial_k},$$

and the matrix H_{jk}^{-1} is the correlated error matrix.

---

*Present address: Science Applications, Inc., Huntsville, Alabama 35805.

[1]J. A. Smith and N. M. Duller, J. Geophys. Res. 64, 2297 (1959).
[2]G. T. Zatsepin and V. M. Kuz'min, Sov. Phys. JETP 12, 1171 (1961).
[3]K. Maeda, Fortschr. Phys. 21, 113 (1973).
[4]W. G. Cantrell, Ph. D. thesis, Texas A & M University, 1969 (unpublished).
[5]H. E. Bergeson, J. W. Keuffel, M. O. Larson, E. R. Martin, and G. Mason, Phys. Rev. Lett. 19, 1487 (1967).
[6]W. R. Sheldon and N. M. Duller, Can. J. Phys. 46, S332 (1968).
[7]W. R. Sheldon, A. R. Bazer-Bachi, G. Vedrenne, C. Dunet, M. Monchant, A. Saint-Marc, W. G. Cantrell, and N. M. Duller, Nucl. Instrum. Methods 111, 133 (1973).
[8]R. Maze, private communication (1968).
[9]W. R. Sheldon, A. R. Bazer-Bachi, J. R. Benbrook, G. Vedrenne, C. Dunet, N. M. Duller, and W. G. Cantrell, in *Proceedings of the Thirteenth International Conference on Cosmic Rays, Denver, 1973* (Colorado Associated Univ. Press, Boulder, 1973), Vol. 3, p. 1715.
[10]A. R. Bazer-Bachi, G. Vedrenne, W. R. Sheldon, and J. R. Benbrook, in *Proceedings of the Fourteenth International Conference on Cosmic Rays, Munich, 1975* (Max Planck Institut für Extraterrestrische Physik, Munich, Germany, 1975), Vol. 6, p. 1886.
[11]S. Miyake, in *Proceedings of the Thirteenth International Conference on Cosmic Rays, Denver, 1973* (Ref. 9), Vol. 5, p. 3638; J. Phys. Soc. Jpn. 18, 1093 (1963).

[12]K. Kobayakawa, in *Proceedings of the Thirteenth International Conference on Cosmic Rays, Denver, 1973* (Ref. 9), Vol. 5, p. 3156.

[13]M. R. Krishnaswamy, M. G. K. Menon, V. S. Narasimham, N. Ito, S. Kawakami, and S. Miyake, Pramana 5, 211 (1975).

[14]G. L. Cassiday, P. C. Gilbert, and D. M. White, Phys. Rev. Lett. 27, 164 (1971).

[15]A. G. Wright, in *Proceedings of the Thirteenth International Conference on Cosmic Rays, Denver, 1973* (Ref. 9), Vol. 3, p. 1709.

[16]H. E. Bergeson, G. W. Carlson, J. W. Keuffel, and J. L. Morrison, in *Proceedings of the Thirteenth International Conference on Cosmic Rays, Denver, 1973* (Ref. 9), Vol. 3, p. 1723.

[17]W. R. Sheldon, W. G. Cantrell, N. M. Duller, F. Cambou, G. Vedrenne, A. R. Bazer-Bachi, A. Saint-Marc, and E. Barouch, Acta Phys. Acad. Sci. Hung. 29, Suppl. 4, 209 (1970).

[18]C. E. Magnusson, J. R. Wayland, and P. J. Green, Phys. Rev. D 6, 2431 (1972).

[19]T. Kitamura, in *Proceedings of the Fourteenth International Conference on Cosmic Rays, Munich, 1975* (Max Planck Institut für Extraterrestrische Physik, Munich, Germany, 1975), Vol. 11, p. 3925.

[20]M. G. K. Menon and P. V. Ramana Murthy, in *Progress in Elementary Particle and Cosmic Ray Physics*, edited by J. G. Wilson and S. A. Wouthuysen (North-Holland, Amsterdam, 1967), Vol. 9 p. 161.

[21]J. C. Barton and C. T. Stockel, Canad. J. Phys. 46, S318 (1968).

[22]A. R. Bazer-Bachi, G. Vedrenne, W. R. Sheldon, and J. R. Benbrook, in *Proceedings of the Fourteenth International Conference on Cosmic Rays, Munich, 1975* (Ref. 19), Vol. 12, p. 4151.

[23]Jay Orear, Notes on Statistics for Physicists, UCRL Report No. 8417, 1958 (unpublished).

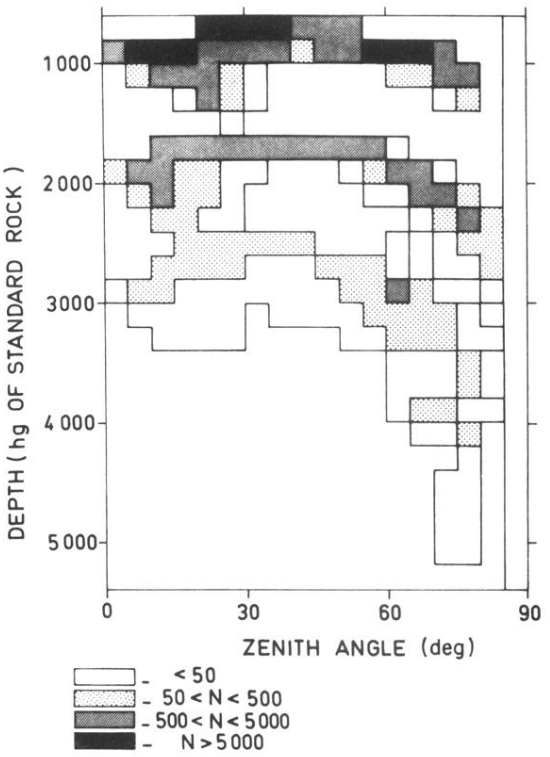

FIG. 1. Distribution of the experimental data as total counts per interval of depth and zenith angle.

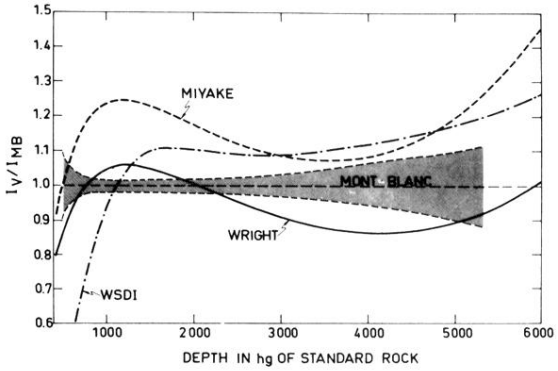

FIG. 3. Comparison of other vertical muon spectra to the present experiment. The shaded region represents the statistical uncertainty in the present experiment as in Fig. 2.